Separation Science and Technology
Publication details, including instructions for authors and subscription information:
http://www.informaworld.com/smpp/title~content=t713708471

Comparison of Fouling Mechanism by $CaSO_4$ and $CaHPO_4$ on Nanofiltration Membranes

Saqib Shirazi[a]; Che-Jen Lin[a]; Simit Doshi[a]; Sumeet Agarwal[a]; Pritesh Rao[a]
[a] Department of Civil Engineering, Lamar University, Beaumont, TX, USA

To cite this Article Shirazi, Saqib , Lin, Che-Jen , Doshi, Simit , Agarwal, Sumeet and Rao, Pritesh(2006) 'Comparison of Fouling Mechanism by $CaSO_4$ and $CaHPO_4$ on Nanofiltration Membranes', Separation Science and Technology, 41: 13, 2861 — 2882
To link to this Article: DOI: 10.1080/01496390600854529
URL: http://dx.doi.org/10.1080/01496390600854529

Separation Science and Technology, 41: 2861–2882, 2006

ISSN 0149-6395 print/1520-5754 online
DOI: 10.1080/01496390600854529

Comparison of Fouling Mechanism by $CaSO_4$ and $CaHPO_4$ on Nanofiltration Membranes

Saqib Shirazi, Che-Jen Lin, Simit Doshi, Sumeet Agarwal, and Pritesh Rao
Department of Civil Engineering, Lamar University, Beaumont, TX, USA

Abstract: We investigated the mechanism of $CaSO_4$ and $CaHPO_4$ scaling on nanofiltration membranes by observing the flux decline behavior. It was found that $CaSO_4$ fouling contributed a greater resistance than $CaHPO_4$ fouling under the same operating conditions. $CaSO_4$ fouling was characterized by reversible cake growth caused by both bulk and surface crystallization at a lower operating pressure, and by surface crystallization at a higher operating pressure. $CaHPO_4$ fouling was characterized by both irreversible pore/surface adsorption and reversible cake growth through surface crystallization regardless of operating conditions. These findings indicate that both fouling solutes and operating parameters should be considered when evaluating inorganic fouling of a nanofilter.

Keywords: Nanofiltration, membrane, inorganic fouling, calcium sulfate, cake formation, bulk and surface crystallization

INTRODUCTION

Membrane filtration is considered as a promising process to provide better drinking water quality (1, 2). Stringent drinking water regulations by the environmental protection agency (EPA) have also triggered the use of membranes in drinking water treatment (3). Four types of membranes are

Received 21 February 2006, Accepted 31 May 2006
Address correspondence to Che-Jen Lin, Department of Civil Engineering, Lamar University, Beaumont, TX 77710-0024, USA. Tel.: (409) 880-8761; Fax: (409) 880-8121; E-mail: jerry.lin@lamar.edu

widely used in drinking water industries; these are microfilter (MF), ultrafilter (UF), nanofilter (NF), and reverse osmosis (RO) (4, 5). Among them, NF has become an attractive option for water softening because of its production of higher water flux, selective rejection of multivalent ions and less operating cost (6–8). Despite these advantages, one of the major limitations of the application of NF in drinking water industries is inorganic fouling (9–15).

Membrane fouling can be reversible or irreversible. Both reversible and irreversible fouling causes permeate flux decline. The flux decline by reversible fouling can be recovered by membrane washing with deionized (DI) water, while the flux decline caused by irreversible fouling cannot be recovered unless the membrane is replaced or cleaned by chemical reagents (9, 16, 17). Reversible fouling occurs due to the formation of cake or gel layer of the foulant on the membrane surface (9, 11), whereas irreversible fouling usually occurs due to strong physisorption and/or chemisorption of solutes onto the membrane surface and its pores (9, 17). The rate and extent of irreversible membrane fouling depends on several factors, such as membrane characteristics (e.g., surface charge, roughness, hydrophobicity), ionic species, temperature, *p*H, and operating conditions (e.g., cross-flow velocity, applied pressure), etc. (15).

During inorganic fouling, a cake is formed on the membrane surface due to the crystallization of inorganic salts (7). Two pathways of crystallization have been reported, i.e., bulk crystallization and surface crystallization. In bulk crystallization, scale forming ions agglomerate due to random collisions of the ions, which develop a crystal that precipitates on the membrane surface. On the other hand, surface crystallization is caused by the lateral growth of crystals on the membrane surface (7). The crystallization process can be affected by various parameters, such as operating conditions, permeate flux, temperature, *p*H, concentration and type of inorganic salt species, and the pretreatment of the feed (e.g., coagulation, flocculation, and sedimentation) (7).

Earlier studies on inorganic fouling have been limited on $CaSO_4$ and $CaCO_3$ (13, 18–22). Although phosphate is an important species that could be present at significant concentrations in raw water, few studies have been performed to investigate the fouling behavior of phosphate salts on NF. In this study, the fouling characteristics and mechanism of $CaHPO_4$ on NF is investigated and compared to $CaSO_4$ fouling under various operating conditions.

MATERIALS & METHODOLOGY

Fouling Model

Fouling increases the resistance and reduces the permeate flux. The relation between the permeate flux and total resistance is described

by equation (1) (17).

$$R_{tot} = \frac{\Delta P - \Delta \pi_m}{\mu J} \tag{1}$$

where J is the permeate flux at a given time (t), ΔP is the applied pressure, $\Delta \pi_m$ is the effective transmembrane osmotic pressure drop caused by increased solute concentration near the membrane surface, μ is the viscosity of the solution, and R_{tot} is the total resistance. R_{tot} is contributed by membrane resistance (R_m), irreversible resistance (i.e. resistance due to pore/surface adsorption) (R_i), reversible cake resistance (R_c), and resistance due to concentration polarization (R_{cp}):

$$R_{tot} = R_m + R_i + R_c + R_{cp} \tag{2}$$

Membrane resistance and irreversible resistance can be determined using pure water filtration where $\Delta \pi_m$ can be ignored for the calculation of R_m and R_i (15, 17):

$$R_m = \frac{\Delta P}{\mu J_0} \tag{3}$$

$$R_i = \frac{\Delta P}{\mu J_f} - R_m \tag{4}$$

where J_0 and J_f are the fluxes of pure water through the clean and fouled membranes.

In addition to fouling, flux can also decline due to increased resistance by concentration polarization (9). The degree of concentration polarization (f), which is the ratio of salt concentration near the membrane surface to bulk concentration, can be estimated as:

$$f = \frac{C_m - C_p}{C_b - C_p} = \exp\left(\frac{J\delta}{D}\right) \tag{5}$$

For $C_p \ll C_b$, equation [5] can be expressed as:

$$f = \frac{C_m}{C_b} = \exp\left(\frac{J\delta}{D}\right) \tag{6}$$

where f is the degree of concentration polarization, J is the solvent flux, C_m, C_p, and C_b are salt concentrations near the membrane surface in the permeate and in the bulk stream, respectively. The ratio of the diffusion coefficient of the salt in the liquid (D) and the boundary layer thickness (δ) is the mass transfer coefficient (k), which can be estimated as follows (23):

$$k = \frac{(J_v)_{salt}}{\ln\left\{\frac{\Delta P}{\pi_b - \pi_p}\left[1 - \frac{(J_v)_{salt}}{(J_v)_{H_2O}}\right]\right\}} \tag{7}$$

where $(J_v)_{salt}$ is the permeate flux from a saline solution, $(J_v)_{H_2O}$ is the permeate flux from the DI water, π_b is the osmotic pressure at the solution bulk concentration, π_p is the osmotic pressure at the permeate. An increased degree of concentration polarization increases the degree of supersaturation (23) [equation (8)] as well as the effective transmembrane osmotic pressure drop ($\Delta\pi_m$) (24) [equation (9)].

$$s/s = f\,\frac{C_b}{C_s} \tag{8}$$

$$\Delta\pi_m = 2C_bRTR_0f \tag{9}$$

where s/s is the degree of supersaturation and C_s is the solute solubility, R is the universal gas constant, T is the absolute temperature, and R_0 is the observed rejection ($1 - C_p/C_b$). The constant "2" (in equation (9) is used for a 1 : 1 electrolyte solution at concentrations where van't Hoff's law is valid, which is the case for the experiments performed in this study. Resistance due to concentration polarization is negligible when the total resistance is dominated by the formation of the cake (25). Under such conditions, the cake resistance due to inorganic fouling can be expressed as followed:

$$R_c = R_{tot} - R_m - R_i \tag{10}$$

Tracey and Davis (16) suggested that the flux decline can be attributed to three major types of fouling, i.e., standard pore blocking, pore blocking, and cake build-up. In standard pore blocking, pores on the membrane are gradually constricted, while the number of available pores remains constant. A standard pore blocking model can be expressed as:

$$R_m + R_i = R_m(1 + K_{SPB}Q_0t)^2 \tag{11}$$

where Q_0 is the initial permeate flow rate and K_{SPB} is the constant for standard pore blocking.

In pore blocking, the number of pores decreases with time due to pore plugging, while the pore size remains constant. The pore blocking model can be expressed as:

$$R_m + R_i = R_m \exp(K_{pB}t) \tag{12}$$

where K_{PB} is the constant for pore blocking.

During cake build-up, no pores are blocked. Instead, the cake resistance increases with time. The cake resistance model can be expressed as:

$$R_{tot} = R_m(1 + 4K_{CB}Q_0^2t)^{1/2} \tag{13}$$

where K_{CB} is the constant for cake build-up.

Since equation (11) is a second-order equation with respect to filtration time, plotting total resistance versus time will produce a concave-up curve if membrane fouling follows standard pore blocking model. Equation (12)

is an exponential equation, therefore, the total resistance versus the time curve also produces a concave-up pattern if the membrane fouling follows the pore blocking model. However, if the cake formation is the predominant fouling mechanism, plotting the total resistance versus time will produce a concave-down pattern according to equations 13 and 16.

Preparation $CaSO_4$ and $CaHPO_4$ Solution

Solutions of $CaSO_4$ (EM Sciences) and $CaHPO_4$ (Fisher Scientific) were prepared by dissolving the salts in deionized (DI) water for 24 hours under magnetic stirring to yield a concentration of 2000 ppm. The *p*H of $CaSO_4$ solution was found to be 6.6 in the feed and remained constant in both the permeate and retentate streams (between 6.5 and 6.7). For $CaHPO_4$ solution, 80 ml of 0.1 M HNO_3 acid was added to adjust the solution *p*H to ca. 3.5 to achieve the 2000 ppm solubility. Before transferring the solutions into the feed tank, the solutions were filtered using a 0.45-μm glass fiber filter (Osmonics) to remove the residual solids. The calcium ion concentration was determined using ion chromatography (Dionex 1000) to verify the feed concentration.

To identify the fouling salt, we performed aqueous speciation calculations using the NIST stability constants for Ca(II)-phosphate system (26). The speciation chart of the $CaHPO_4$ solution from *p*H 1 to 7 is shown in Table 1. Under our experimental conditions, the aqueous speciation in the feed solution at *p*H 3.5 is dominated by Ca^{2+} and $H_2PO_4^-$, with the precipitating salt as $CaHPO_4$. The solubility product of $CaHPO_{4(s)}$ is $10^{-6.9}$ and the product of Ca^{2+} and HPO_4^{2-} in Table 1 at *p*H 3.5 is $10^{-7.28}$, which is at a near-saturation condition. The precipitation of $Ca_3(PO_4)_2$ is not likely due to the very low PO_4^{3-} concentration at the experimental *p*H. During filtration, the *p*H of $CaHPO_4$ solution remained relatively constant in both the permeate and the retentate the streams (between 3.3 and 4.5). The slight *p*H change may be due to the precipitation of $CaHPO_4$, which caused a small shift in the aqueous speciation.

Measurement of Concentration Polarization

In order to measure the effect of concentration polarization (CP) during the $CaSO_4$ and $CaHPO_4$ filtration on NF, 1500 ppm of $CaSO_4$ and 1500 ppm of $CaHPO_4$ (at *p*H 3.5) were prepared and filtered through the NF membranes at different operating pressures (345 and 966 KPa) and cross-flow velocities (3.2×10^{-3} m/s and 4.0×10^{-2} m/s). During the filtration, there was a lag phase prior to scaling when CP caused the permeate flux decline, and the degree of CP was calculated using equations (5–8).

Table 1. Speciation diagram for the feed solution at different *p*H. Only the important species are shown. Both total calcium and phosphate concentrations are 0.015 M. The stability constants used are based on Smith and Martell 2004. The initial *p*H of the feed was maintained at 3.5 and the *p*H remained relatively constant throughout the filtration.

Species *p*H	H_3PO_4 (M)	$H_2PO_4^-$ (M)	HPO_4^{2-} (M)	PO_4^{3-} (M)	Ca^{2+} (M)	$CaHPO_4$ (M)	$CaH_2PO_4^+$ (M)	$CaOH^+$ (M)
1	1.28×10^{-2}	1.54×10^{-3}	1.85×10^{-9}	2.80×10^{-20}	1.45×10^{-2}	1.99×10^{-9}	5.00×10^{-4}	1.32×10^{-14}
2	5.88×10^{-3}	7.07×10^{-3}	8.50×10^{-8}	1.29×10^{-17}	1.30×10^{-2}	8.16×10^{-8}	2.05×10^{-3}	1.18×10^{-13}
3	8.99×10^{-4}	1.08×10^{-2}	1.30×10^{-6}	1.97×10^{-15}	1.21×10^{-2}	1.16×10^{-6}	2.92×10^{-3}	1.10×10^{-12}
4	9.82×10^{-5}	1.18×10^{-2}	1.42×10^{-5}	2.15×10^{-13}	1.19×10^{-2}	1.25×10^{-5}	3.13×10^{-3}	1.08×10^{-11}
5	9.69×10^{-6}	1.16×10^{-2}	1.40×10^{-4}	2.12×10^{-11}	1.18×10^{-2}	1.22×10^{-4}	3.08×10^{-3}	1.08×10^{-10}
6	8.44×10^{-7}	1.01×10^{-2}	1.22×10^{-3}	1.85×10^{-9}	1.14×10^{-2}	1.03×10^{-3}	2.59×10^{-3}	1.04×10^{-9}
7	3.77×10^{-8}	4.53×10^{-3}	5.45×10^{-3}	8.25×10^{-8}	9.96×10^{-3}	4.03×10^{-3}	1.01×10^{-3}	9.09×10^{-9}
3.5	3.04×10^{-4}	1.16×10^{-2}	4.40×10^{-6}	2.11×10^{-14}	1.19×10^{-2}	3.88×10^{-6}	3.09×10^{-3}	3.43×10^{-12}

Experimental Protocol

A polyamide flat sheet NF membrane (HL, Osmonics, Minnetonka, MN) was used throughout the study. This is a thin-film membrane that can tolerate *p*H 3-9 at 25°C. According to the manufacturer's specification, the typical flux for this membrane is 39 GFD (gallon/ft^2/day) at 100 psi (i.e. 1.83×10^{-5} $m^3/m^2/s$ at 690 KPa). We selected this membrane due to its higher permeate flux compared to most other commercially available nanofilters. The Sepa-CF cell (Osmonics, Minnetonka, MN) was used with a width of 0.095 m, channel length of 0.146 m, and channel height of 8.60×10^{-4} m, which produced the membrane surface area of 0.014 m^2. A plastic sieve-type feed spacer was placed inside the cavity on the feeding side of the membrane. A schematic diagram of the apparatus is shown in Fig. 1. The experiments were carried out at room temperature (23–25°C) in a complete recirculation mode in which both the permeate and the retentate streams were recirculated back to the feed tank.

A calcium ion selective probe (Orion, Model 97–20) was placed inside the feed solution to continuously monitor Ca^{2+} concentration in the feed tank. During filtration, as the salt crystals deposited at the membrane surface, a slight change of the feed concentration was observed, which was minimized by adding saturated solutions into the feed tank to maintain a feed concentration of 2000 $\pm$ 50 ppm. The cross-flow velocity of the experiments was changed by adjusting the pump speed. A 0.45-μm glass fiber filter (Osmonics) was used in the retentate side for selected experiments, when the bulk crystals were intended to be removed from the system. Before each experiment, the nanofilter was stabilized overnight with deionized (DI) water at 3.2×10^{-3} m/s cross-flow velocity and 345 KPa operating pressure. At the start of each run, the membrane permeability was

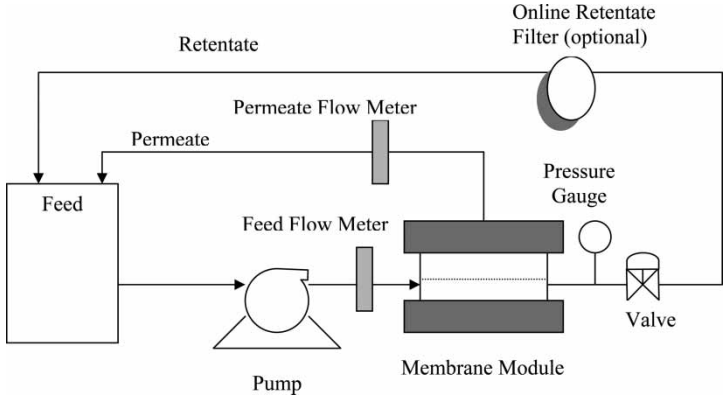

Figure 1. Schematics of experimental setup.

determined with DI water. Only those membranes that gave permeability within the 95% confidence interval were used.

A gear pump (Tuthill Corporation) was used to pump the feed from the feed tank to the membrane module. Two flow meters (Cole Parmer GR8000) were used to measure the feed and permeate flow rates. Feed water recovery was measured by the ratio of permeate flow rate to feed flow rate. Permeate flux was calculated as the ratio of permeate flow rate to the membrane area. A pressure gauge (Cole-Palmer, U-68950-10) was used to determine the operating pressure, and a needle valve (Cole-Palmer) was used on the retentate side to control operating pressure. Fouling was observed through the decline of the permeate flux. A new membrane sheet was used for filtration until the permeate flux reached a steady state where no further flux decline was observed.

Membrane Washing

After each filtration cycle, the membrane was washed with DI water to determine the fouling reversibility. During washing, membranes were removed from the membrane module, rinsed with DI water to remove the reversible portion of the cake from the membrane surface. After rinsing thoroughly with DI water, the membrane was reinserted into the membrane module, and washed for six more hours by passing the DI water through the feed side.

RESULTS AND DISCUSSION

Fouling Behavior of $CaSO_4$ and $CaHPO_4$

Unlike other salts, during $CaSO_4$ fouling on NF, the permeate flux decline remains unaltered for a considerable period of time before the fouling starts (7, 20). Lin et al. (9) verified the pattern of $CaSO_4$ fouling on NF by a four-stage (concentration polarization, nucleation, active fouling due to cake formation, and steady-state filtration) mechanistic model. In this study, we compared the fouling behavior between $CaSO_4$ and $CaHPO_4$.

First, 2000 ppm of $CaSO_4$ and 2000 ppm of $CaHPO_4$ were filtered at 3.2×10^{-3} m/s cross-flow velocity and 345 KPa operating pressure. The results are shown in Fig. 2. During $CaSO_4$ fouling on NF, after concentration polarization, the permeate flux decline remained unaltered for 4.5 hrs. At this stage, $CaSO_4$ molecules aggregated and formed nuclei (nucleation stage). Once sufficient nuclei were formed, they deposited onto the membrane surface and reduced the permeate flux significantly (cake formation stage). However, during $CaHPO_4$ filtration, the nucleation stage was not present (Fig. 2), which might be due to the different nucleation kinetics of $CaSO_4$

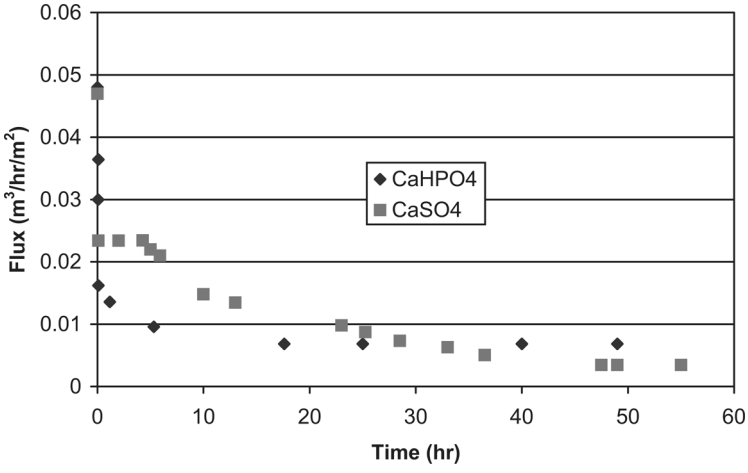

Figure 2. $CaSO_4$ and $CaHPO_4$ Fouling at 3.2×10^{-3} m/s and 345 KPa.

and $CaHPO_4$ (27). Nucleation occurs slowly for $CaSO_4$ fouling but rapidly for $CaHPO_4$ fouling, leading to direct $CaHPO_4$ solids on the membrane surface.

Furthermore, a 70% and 90% of flux decline was observed during the filtration of $CaHPO_4$ and $CaSO_4$, respectively (Fig. 2). Such flux reduction was caused by a combination of concentration polarization and inorganic fouling. It took 18 hrs for the system to reach a steady state stage for $CaHPO_4$, and 48 hrs for $CaSO_4$. At the steady state (after the 40^{th} hour), total resistances caused by $CaSO_4$ and $CaHPO_4$ were 3.8×10^{14} m^{-1} and 1.4×10^{14} m^{-1}, based on equation (1). $CaSO_4$ scales produce greater resistance than $CaHPO_4$ scales under the same operating conditions.

Characteristics of Fouling by $CaSO_4$ and $CaHPO_4$

To investigate the reversibility of $CaSO_4$ and $CaHPO_4$ fouling on NF, two separate experiments were performed at 3.2×10^{-3} m/s and 345 KPa using near saturated (2000 ppm) concentration of $CaSO_4$ and $CaHPO_4$ solutions as feed. Then we compared the membrane permeability before and after membrane washing in each filtration cycle. The results are plotted in Figs. 3a and 3b.

The permeability of the washed membrane after $CaSO_4$ and $CaHPO_4$ fouling was 0.0001 and 9.0×10^{-5} $m^3/hr/m^2/KPa$, respectively (the permeability of the new membrane was 0.0001 $m^3/hr/m^2/KPa$). The permeation flux is significantly reduced after the washing (ca. 25–30%) for $CaHPO_4$ filtration. Statistical tests (paired T-test) were performed to test the difference in permeability between the new and the washed membrane. For $CaSO_4$ filtration, we found no statistical difference at 5% significance level in the

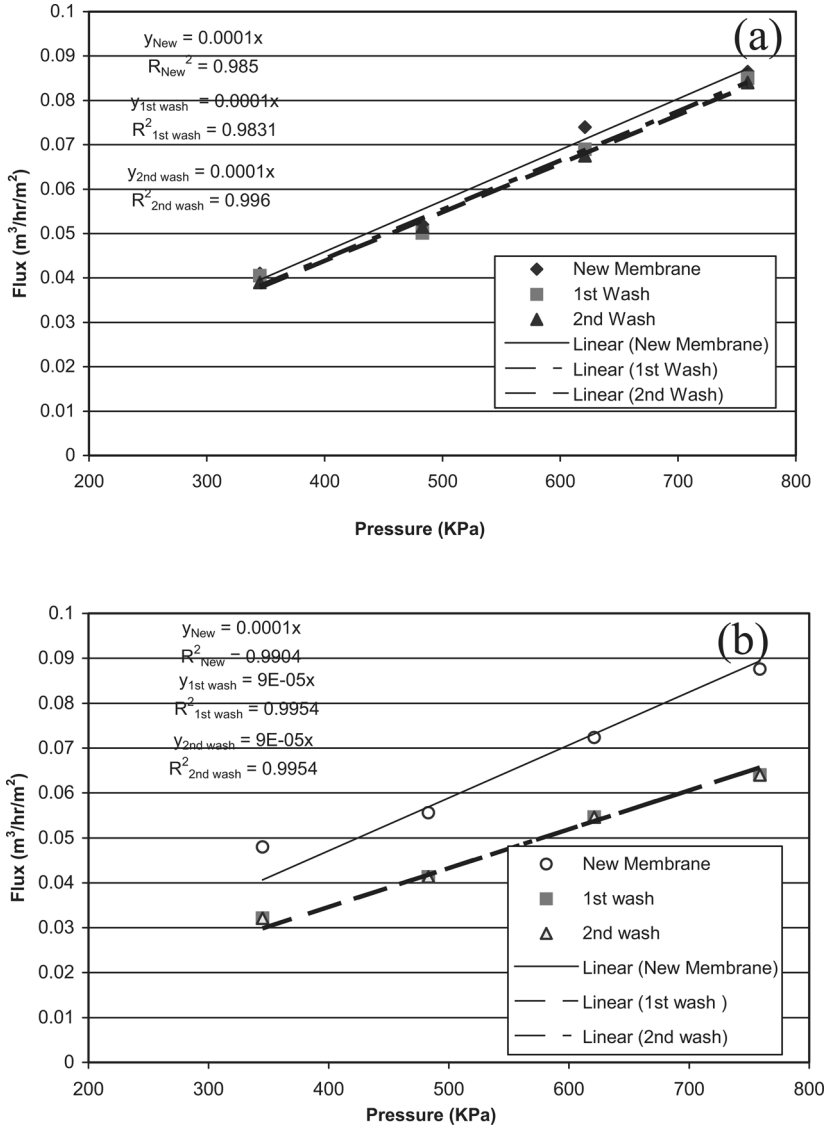

Figure 3. Membrane permeability for new and washed membranes for (a) $CaSO_4$ filtration and (b) $CaHPO_4$ filtration.

three data sets ($p = 0.79$). Since the initial permeate flux and permeability were recovered completely after removing the $CaSO_4$ scale by washing with DI water, it appears that the reversible cake formation is responsible for the flux decline in $CaSO_4$ filtration. The paired T-test was also performed for the flux data for $CaHPO_4$ filtration. A significant difference

in the permeability ($p = 0.002$) was found, indicating that a portion of $CaHPO_4$ solids might be adsorbed on the pore/surface of NF during $CaHPO_4$ filtration. This leads to irreversible fouling and cannot be recovered by washing with DI water.

To verify the fouling characteristics of $CaSO_4$ and $CaHPO_4$, 2000 ppm of $CaSO_4$ and $CaHPO_4$ solutions were filtered at various pressures (345 and 966 KPa) and cross-flow velocities (3.2×10^{-3} and 4.0×10^{-2} m/s). Their filtration cycles are shown in Fig. 4a and 4b. Regardless of the operating condition, the initial fluxes were fully recovered after washing with DI water for $CaSO_4$ filtration (Fig. 4a). For $CaHPO_4$ filtration (Fig. 4b), the initial flux was not recovered after the same membrane washing procedure. This indicates that an irreversible pore/surface blockage of NF has occurred. We further estimate the magnitude of resistance terms caused by the reversible cake and irreversible pore/surface blockage after the completion of the filtration cycle for $CaSO_4$ and $CaHPO_4$.

The ultimate reversible cake resistance of $CaSO_4$ fouling at various operating parameters was quantified using equations (1–9), and shown in Table 2. At constant operating pressure (345 KPa), reversible cake resistance was higher at lower cross-flow velocity. At 3.2×10^{-3} and 4.0×10^{-2} m/s of cross-flow velocity, the ultimate reversible cake resistance was 3.8×10^{14} and 3.5×10^{14} m^{-1}. A higher cross-flow velocity created a greater shear flow on the retentate side, which produced a thinner cake. Moreover, lower feed water recovery at the higher cross-flow velocity produced a lower supersaturation index (3.96 at 3.2×10^{-3} m/s and 3.35 at 4.0×10^{-2} m/s). This in turn formed a less compact cake on the membrane surface that resulted in lower resistance (4). At constant cross-flow velocity (4.0×10^{-2} m/s), the resistance due to cake formation was higher at a higher operating pressure (966 KPa). The ultimate cake resistances at 345 KPa and 966 KPa were found to be 3.8×10^{14} m^{-1} and 1.0×10^{15} m^{-1}, respectively. The higher operating pressure increased the feed water recovery and degree of supersaturation (3.35 at 345 KPa and 15.2 at 966 KPa) near the membrane surface.

The resistance due to pore/surface adsorption (R_i) for $CaHPO_4$ fouling was calculated using equations (1–4), and shown in Table 3. At constant operating pressure (345 KPa), R_i at 3.2×10^{-3} and 1.0×10^{-2} m/s were 3.89×10^{13} and 2.89×10^{13} m^{-1}, respectively. At constant cross-flow velocity (1.0×10^{-2} m/s), R_i were 2.89×10^{13} and 4.35×10^{13} m^{-1} at 345 and 966 KPa, respectively. These results suggest that the resistance due to pore/surface adsorption strongly depends on operating parameters. At constant cross-flow velocity, a higher operating pressure produced a greater convective flux towards the membrane, which resulted in more pore/surface adsorption and thus a greater irreversible resistance. At constant operating pressure, higher cross-flow velocity allowed less salt to be adsorbed, which lowered the irreversible resistance.

The ultimate resistance caused by the reversible cake of $CaHPO_4$ was calculated using equations (1–4) and [10], and sown in Table 4. The ultimate

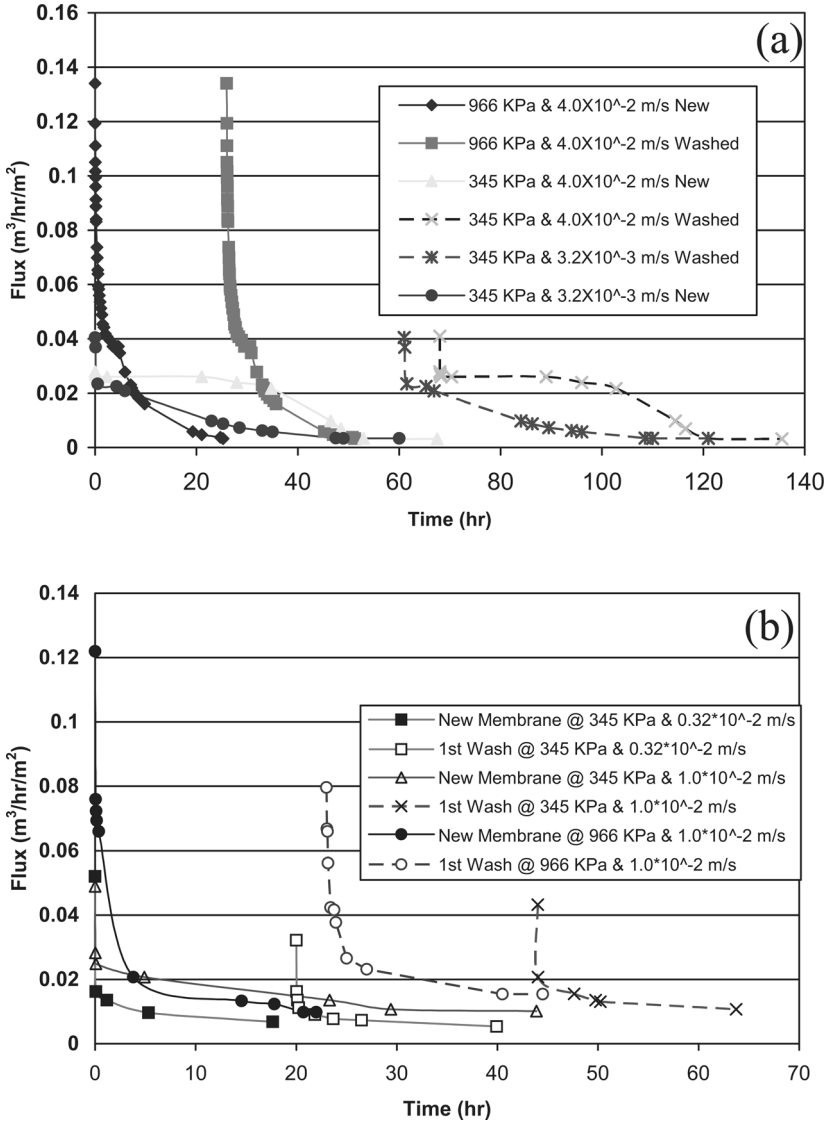

Figure 4. Flux change during (a) $CaSO_4$ filtration and (b) $CaHPO_4$ filtration at various operating parameters.

reversible cake resistance was $7.36 \times 10^{13}\,m^{-1}$ at 3.2×10^{-3} m/s and 345 KPa; $3.85 \times 10^{13}\ m^{-1}$ at 1.0×10^{-2} m/s and 345 KPa; and $2.5 \times 10^{14}\ m^{-1}$ at 1.0×10^{-2} m/s and 966 KPa. At constant operating pressure (345 KPa), a higher cross-flow velocity led to a lower cake resistance because of the lower feed water recovery and greater shear flow. At constant cross-flow velocity

Table 2. Ultimate reversible cake resistance (R_c) during $CaSO_4$ fouling on NF at different operating parameters

Constant operating pressure (345 KPa)		Constant cross-flow velocity (4.0×10^{-2} m/s)	
Cross-flow velocity	Cake resistance	Operating pressure	Cake resistance
3.2×10^{-3} m/s	3.8×10^{14} m^{-1}	345 KPa	3.8×10^{14} m^{-1}
4.0×10^{-2} m/s	3.5×10^{14} m^{-1}	966 KPa	1.0×10^{15} m^{-1}

(1.0×10^{-2} m/s), a higher operating pressure caused a higher cake resistance because of the increased recovery and degree of concentration polarization.

It can be seen from Tables 3 and 4 that the ultimate resistance of $CaHPO_4$ cake was much higher than its irreversible resistance, indicating that much of the $CaHPO_4$ fouling was also caused by reversible cake formation. Using the flux data in Figs. 2 and 4b, the total resistance (R_{tot}) were calculated at different operating conditions using equation (1) and plotted against time in Fig. 5. All case produced concave-down curves suggesting cake formation as the predominant fouling mechanism (according to equations (11–13) (16). Comparing the cake resistance at different cross-flow velocities and operating pressures in Tables 2, 3, and 4, the resistance was much more sensitive to change in operating pressure compared to the change in cross-flow velocity.

Mechanism of Fouling by $CaSO_4$ and $CaHPO_4$

During inorganic fouling, the cake can be formed in one of three mechanisms (10):

1. by bulk crystallization only
2. by surface crystallization only
3. by both bulk and surface crystallization

Table 3. Irreversible resistance (R_i) during $CaHPO_4$ fouling on NF at different operating parameters

Constant operating pressure (345 KPa)		Constant cross-flow velocity (1.0×10^{-2} m/s)	
Cross-flow velocity	Resistance	Operating pressure	Resistance
3.2×10^{-3} m/s	3.89×10^{13} m^{-1}	345 KPa	2.89×10^{13} m^{-1}
1.0×10^{-2} m/s	2.89×10^{13} m^{-1}	966 KPa	4.35×10^{13} m^{-1}

Table 4. Ultimate reversible cake resistance (R_c) during $CaHPO_4$ fouling on NF at different operating parameters

Constant operating pressure (345 KPa)		Constant cross-flow velocity (1.0×10^{-2} m/s)	
Cross-flow velocity	Cake resistance	Operating pressure	Cake resistance
3.2×10^{-3} m/s	7.36×10^{13} m^{-1}	345 KPa	3.85×10^{13} m^{-1}
1.0×10^{-2} m/s	3.85×10^{13} m^{-1}	966 KPa	2.49×10^{14} m^{-1}

It has also been suggested by Hoek et al. that a greater degree of concentration polarization promotes surface crystallization (24). Lee and Lee (7) showed that a lower degree of concentration polarization promotes both bulk and surface crystallization in $CaSO_4$ fouling. We performed additional experiments to elucidate the cake formation mechanism of $CaSO_4$ and $CaHPO_4$.

Fouling Mechanism of $CaSO_4$ and $CaHPO_4$ at Constant Cross-flow Velocity

To study the mechanism of $CaSO_4$ fouling at constant cross-flow velocity (4.0×10^{-2} m/s), 2000 ppm of $CaSO_4$ was filtered by varying the operating pressure at 345 KPa and 966 KPa. In each case, >90% rejection of $CaSO_4$ was observed. To assess if bulk crystallization was responsible

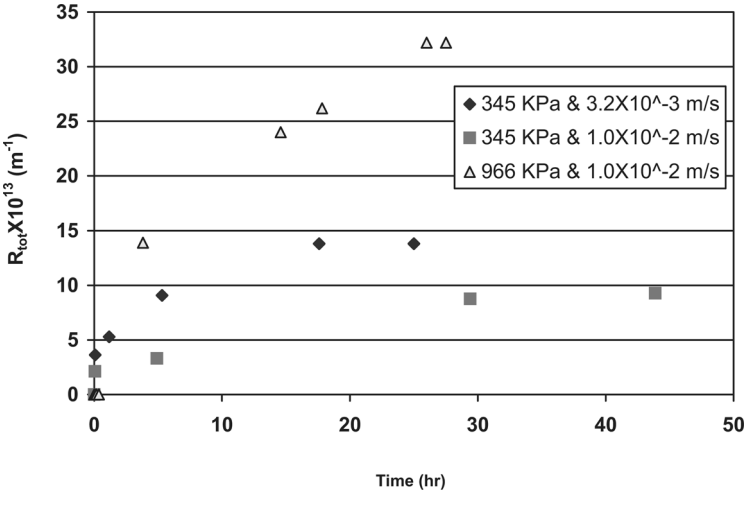

Figure 5. Total resistance versus time during $CaHPO_4$ filtration.

for the fouling, filtration experiments were performed with and without the addition of an inline retentate filter (Fig. 1). A 0.45-μm pore size filter was placed in the retentate side to remove bulk crystals from the system (10). The results are shown in Fig. 6a.

For $CaSO_4$ fouling at 345 KPa and 4.0×10^{-2} m/s, the ultimate flux at steady state was higher when the inline retentate filter was in place (0.01 versus 0.003 $m^3/hr/m^2$). A higher ultimate flux with inline retentate filter indicates that the added filter reduced cake growth on membrane surface. The nucleation period is clearly shorter without the inline filter (e.g., 24 versus 34 hrs, Fig. 6a). Moreover, the filtration took longer to reach the steady state when the filter was in place (e.g., 80 versus 60 hrs). This indicates that the $CaSO_4$ cake formation was enhanced when bulk crystals were not removed, and that bulk crystallization should be one of the mechanisms for $CaSO_4$ crystallization at 345 KPa and 4.0×10^{-2} m/s.

Furthermore, since the inline filter removes the bulk crystals only, the cake would not be formed considerably (thus no significant flux reduction after the concentration polarization stage) if bulk crystallization would had been the only mechanism for the cake formation during $CaSO_4$ fouling. However, a significant flux reduction with the inline filter was also observed (Fig. 6a). This indicates that the formation of the cake also occurred at the membrane surface. Therefore, we conclude that both bulk and surface crystallization were responsible for cake formation in $CaSO_4$ fouling on NF at 345 KPa and 4.0×10^{-2} m/s. This result agrees with the finding of Lee and Lee (7) where they suggested that at a lower operating pressure the mechanism of $CaSO_4$ fouling is contributed by both the bulk and the surface crystallization.

When the operating pressure was increased from 345 KPa to 966 KPa, the degree of concentration polarization changed from 4.52 to 16.0 (Table 5). However, little difference in the ultimate flux, nucleation period, and the time to reach the steady state was observed with and without the retentate filter, i.e., the filter had little effect on $CaSO_4$ fouling at this operating pressure (Fig. 6a). If bulk crystals are formed at 4.0×10^{-2} m/s and 966 KPa (where initial feed water recovery was only 17% and reduced further due to the flux decline by fouling), the crystals should be removed by the inline filter and there should be a significant difference in the fouling pattern with and without the filter. Based on the very short nucleation period and little difference in the fouling pattern, the mechanism for $CaSO_4$ fouling under a high operating pressure should be dominated by surface crystallization. Similar results were also reported by Song and Elimelech (28).

To investigate the fouling mechanism of $CaHPO_4$, 2000 ppm of $CaHPO_4$ was filtered at a constant cross-flow velocity (1.0×10^{-2} m/s) by varying the operating pressure at 345 and 966 KPa. The results are shown in Fig. 6b. At 1.0×10^{-2} m/s and 345 KPa, the initial degree of concentration polarization was estimated to be 4.80 (Table 5). At this condition, the ultimate flux was

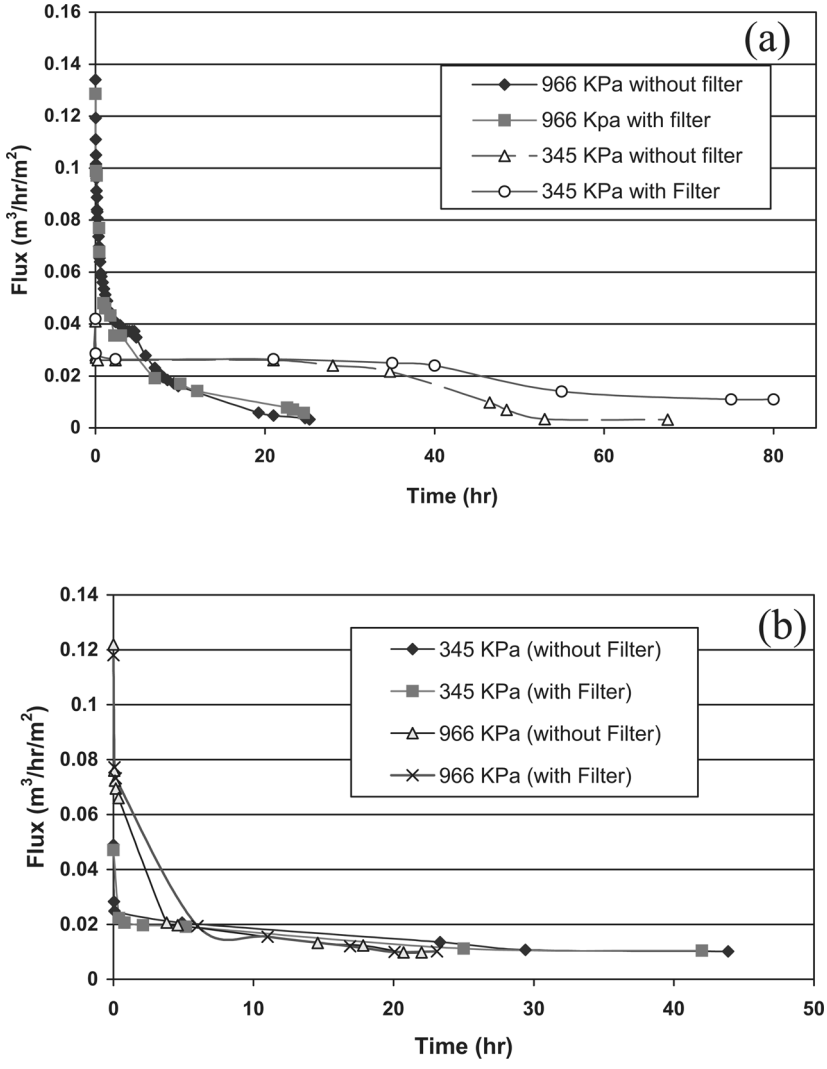

Figure 6. Flux versus time at constant cross-flow velocity: (a) $CaSO_4$ filtration at 4.0×10^{-2} m/s (b) $CaHPO_4$ filtration at 1.0×10^{-2} m/s. The experiments at high pressure were stopped at about the 25 hour since the flux did not vary significantly after three consecutive readings.

almost the same ($0.01\ m^3/hr/m^2$) with or without the retentate filter. Moreover, the inline filter had little effect on the cake growth and the filtration period during $CaHPO_4$ fouling (Fig. 6b). This suggests that the mechanism of fouling by $CaHPO_4$ was due to surface crystallization under the operating conditions.

Table 5. Degree of concentration polarization (CP) and osmotic pressure at membrane all for 1500 ppm $CaSO_4$ and 1500 ppm $CaHPO_4$ at various operating condition

Salt species	Operating parameters	Flux for DI-water ($m^3/hr/m^2$)	Flux for salt soln. ($m^3/hr/m^2$)	Mass transfer coef. (k) (m/hr) Eq. (7)	Degree of CP (f) Eq. (6)
$CaSO_4$	3.2×10^{-3} m/s & 345 KPa	0.05	0.024	0.0168	4.16
	4.0×10^{-2} m/s & 345 KPa	0.05	0.028	0.0222	3.52
	4.0×10^{-2} m/s & 966 KPa	0.14	0.040	0.0144	16.0
$CaHPO_4$	3.2×10^{-3} m/s & 345 KPa	0.05	0.018	0.0110	5.12
	1.0×10^{-2} m/s & 345 KPa	0.05	0.020	0.0127	4.80
	4.0×10^{-2} m/s & 345 KPa	0.05	0.032	0.0302	2.88
	1.0×10^{-2} m/s & 966 KPa	0.14	0.018	0.0061	19.5

At the same cross-flow velocity, when the operating pressure was changed from 345 KPa to 966 KPa, the degree of concentration polarization was changed from 4.80 to 19.5 (Table 5). At such a high operating pressure, the rate of crystallization could be so high that the formation of salt crystals started instantaneously at the membrane surface. This minimized the effect of bulk crystallization (if any) on the flux decline during $CaHPO_4$ fouling on NF. As seen from Fig. 6b, the ultimate flux remained almost same ($0.009\ m^3/hr/m^2$) with and without online retentate filter.

Fouling Mechanism of $CaSO_4$ and $CaHPO_4$ at Constant Operating Pressure

Solutions containing 2000 ppm of $CaSO_4$ were filtered at 345 KPa at various cross-flow velocities at 3.2×10^{-3} and 4.0×10^{-2} m/s to investigate the fouling mechanism. The results are plotted in Fig. 7a. The degree of concentration polarization was found to be 4.16 (at 3.2×10^{-3} m/s) and 3.52 (at 4.0×10^{-2} m/s), respectively (Table 5). The ultimate flux with and without the inline filter was $0.01\ m^3/hr/m^2$ and $0.003\ m^3/hr/m^2$ at 3.2×10^{-3} m/s crossflow velocity, indicating that the added filter reduced the cake growth on the membrane (thus a greater flux). Figure 7a also shows that the nucleation

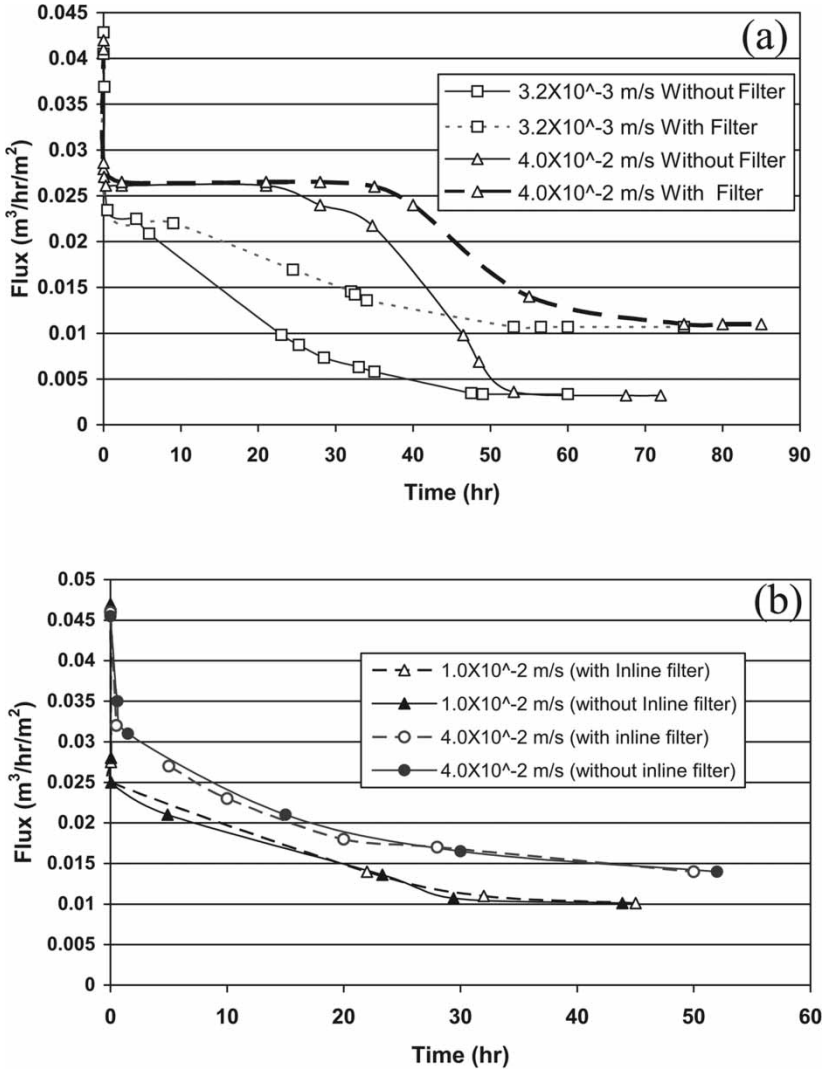

Figure 7. Flux versus time at constant operating pressure (345 KPa) (a) $CaSO_4$ filtration (b) $CaHPO_4$ filtration.

period is clearly shorter without the inline filter (4.5 versus 9 hrs), and the filtration took longer to reach a steady state when the filter was in place (57 hrs versus 49 hrs). This indicates that $CaSO_4$ cake formation was enhanced by bulk crystals, and bulk crystallization should be one of the mechanisms for $CaSO_4$ fouling. At 4.0×10^{-2} m/s crossflow velocity, there is a significant difference in the ultimate flux (0.01 versus 0.003 $m^3/hr/m^2$), nucleation period (34 versus 24 hrs), and filtration to reach the steady state (80 versus 60 hrs).

This indicates that both bulk and surface crystallizations were responsible for the cake formation under the experimental conditions.

Solutions containing 2000 ppm $CaHPO_4$ were also filtered at the same operating pressure (345 KPa) and different cross-flow velocities (1.0×10^{-2} and 4.0×10^{-2} m/s). The degree of concentration polarization was found to be 4.80 (1.0×10^{-2} m/s) and 2.88 (4.0×10^{-2} m/s) (Table 5). The results are plotted in Fig 7b. It can be seen that the inline filter had little effect on cake growth, ultimate flux, and the filtration time during the $CaHPO_4$ fouling at 345 KPa. Based on the observations, we concluded that the primary mechanism for the $CaHPO_4$ fouling should be surface crystallization.

During $CaHPO_4$ fouling at 345 KPa and 4.0×10^{-2} m/s cross-flow velocity, the degree of concentration polarization was only 2.88, which is lower than the value of 4.16 for $CaSO_4$ at 3.2×10^{-3} m/s (at which bulk crystallization is one primary mechanism of fouling during $CaSO_4$ fouling). Even at this lower degree of concentration polarization, the cake formation was contributed only by surface crystallization during $CaHPO_4$ fouling on NF. Figures 6 and 7 reveal that operating parameters (cross-flow velocity and operating pressure, etc.) as well as the type of fouling solutes strongly affect the mechanism and rate of cake formation, either by surface crystallization, bulk crystallization, or by both bulk and surface crystallization.

CONCLUSIONS

This study was performed to compare the fouling behavior and mechanism of $CaSO_4$ and $CaHPO_4$ fouling on NF. The results showed that the flux decline caused by $CaSO_4$ fouling was due to reversible cake formation, while the flux decline caused by $CaHPO_4$ fouling was partially irreversible by both pore/surface adsorption and cake formation. The mechanism of fouling depends both on operating parameters and the types of fouling salt. For the $CaSO_4$ filtration, the fouling was contributed by both bulk and surface crystallization at a lower operating pressure and by surface crystallization only at a higher operating pressure. For $CaHPO_4$ filtration, the primary fouling mechanism was through surface crystallization regardless of operating conditions. These findings indicate that the fouling salts in feed water as well as operating conditions of filtration needs to be considered while evaluating inorganic fouling on nanofilters.

SYMBOLS

C_b	Salt concentration at the bulk (kg/m^3)
C_m	Salt concentration at the membrane surface (kg/m^3)
C_p	Salt concentration in the permeate (kg/m^3)
C_s	Solubility of the species

D	Diffusion coefficient of the salt (m^2/hr)
f	Degree of concentration polarization
J	Permeate flux ($m^3/hr/m^2$)
J_0	Initial permeate flux ($m^3/hr/m^2$)
J_f	Flux of deionized water through the fouled membrane ($m^3/hr/m^2$)
k	Mass transfer coefficient (m/hr)
K_{SPB}	Constant for standard pore blocking
K_{PB}	Constant for pore blocking
K_{CB}	Constant for cake build-up
N_R	Reynolds Number
t	Time (s)
T	Temperature (K)
R_0	Observed rejection
R_m	Membrane resistance (m^{-1})
R_{cp}	Resistance due to concentration polarization (m^{-1})
R_c	Cake resistance (m^{-1})
R_i	Irreversible resistance (m^{-1})
R_{tot}	Total resistance (m^{-1})
s/s	Degree of supersaturation
V	Cross-flow velocity (m/s)
ΔP	Applied pressure (KPa)
$\Delta\pi_m$	Effective transmembrane osmotic pressure drop (KPa)
μ	Dynamic viscosity of solution ($Kg/m/hr$)
ν	Kinematic viscosity of solution (m^2/hr)

ACKNOWLEDGEMENTS

This study was funded in part by the Texas State University System's (TSUS) Sustainable Agricultural Water Conservation (SAWC) Program funded by the USDA through Sul Ross University, and by the Texas Hazardous Waste Research Center (THWRC). The financial support from the funding agencies is gratefully acknowledged. We would also like to thank the anonymous reviewers for their helpful comments in the review process.

REFERENCES

1. Lee, N., Amy, G., Croue, J.P., and Buisson, H. (2004) Identification and understanding of fouling in low-pressure membrane (MF/UF) filtration by natural organic matter (NOM). *Water Research*, 38: 4511–4523.
2. Koo, T., Lee, Y.J., and Sheikholeslami, R. (2001) Silica fouling and cleaning of reverse osmosis membranes. *Desalination*, 139: 43–56.
3. Kilduff, J.E., Mattaraj, S., and Belfort, G. (2004) Flux decline during nanofiltration of naturally-occurring dissolved organic matter: effects of osmotic pressure,

membrane permeability, and cake formation. *Journal of Membrane Science*, 239: 39–53.
4. Lin, C.J., Shirazi, S., Rao, P., and Agarwal, S. (2006) Effect of operating parameters on cake formation of $CaSO_4$ in nanofiltration. *Water Research*, 40: 806–816.
5. Bilstad, T. (1997) Membrane operations. *Water Science and Technology*, 36: 17–24.
6. Lin, C.J., Rao, P., and Shirazi, S. (2004) Effect of operating parameters on permeate flux decline caused by cake formation—a model study. *Desalination*, 171: 95–105.
7. Lee, S. and Lee, C. (2000) Effect of operating conditions on $CaSO_4$ scale formation mechanism in nanofiltration for water softening. *Water Research*, 34 (15): 3854–3866.
8. Sharma, R.R., Agrawal, R., and Chellam, S. (2003) Temperature effects on sieving characteristics of thin-film composite nanofiltration membranes: pore size distributions and transport parameters. *Journal of Membrane Science*, 223: 69–87.
9. Lin, C.J., Shirazi, S., and Rao, P. (2005) A mechanistic model for $CaSO_4$ fouling in nanofiltration. *Journal of Environmental Engineering*, 131: 1387–1392.
10. Lee, S., Kim, J., and Lee, C. (1999) Analysis of $CaSO_4$ scale formation mechanism in various nanofiltration modules. *Journal of Membrane Science*, 163: 63–74.
11. Speth, T.F., Summers, R.S., and Guesses, A.M. (1998) Nanofiltartion foulants from a treated surface water. *Environmental Science and Technology*, 32: 3612–3617.
12. Rabie, H.R., Cote, P., and Adams, N. (2001) A method for assessing membrane fouling in pilot and full scale systems. *Desalination*, 141: 237–243.
13. Le Goueleec, Y.A. and Elimelech, M. (2002) Calcium sulfate (gypsum) scaling in nanofiltration of agricultural drainage water. *Journal of Membrane Science*, 5310: 1–13.
14. Shaalan, H.F. (2002) Development of fouling control strategies pertinent to nanofiltration membranes. *Desalination*, 153: 125–131.
15. Jones, K.L. and O'Melia, C.R. (2001) Ultrafiltration of protein and humic substances: effect of solution chemistry on fouling and flux decline. *Journal of Membrane Science*, 193: 163–173.
16. Tracey, E.M. and Davis, R.H. (1994) Protein adsorption of track-etched polycarbonate microfiltration membranes. *Journal of Colloids and Interface Science*, 167: 104.
17. Fabish, R.F. and Cohen, Y. (2001) Fouling and rejection behavior of ceramic and polymer-modified ceramic membranes for ultrafiltration of oil-in-water emulsions and microemulsions. *Colloids and Surfaces A: Physicochemical and Engineering Aspects*, 191: 27–40.
18. Van der Bruggen, B., Braeken, L., and Vandecasteele, C. (2002) Flux decline in nanofiltration due to adsorption of organic compounds. *Separation and Purification Technology*, 29: 23–31.
19. Hasson, D., Drak, A., and Semiat, R. (2001) Inspection of $CaSO_4$ scaling on RO membranes at various water recovery levels. *Desalination*, 139: 73–81.
20. Bhattacharjee, S. and Johnston, G. (2002) A model of membrane fouling by salt precipitation from multicomponent ionic mixtures in cross-flow nanofiltration. *Environmental Engineering Science*, 19: 399–412.
21. Gilron, J. and Hasson, D. (1987) Calcium sulfate fouling of reverse osmosis membranes: flux decline mechanism. *Chemical Engineering Science*, 42 (10): 2351–2360.

22. Le Gouellec, Y.A. and Elimelech, M. (2002) Control of calcium sulfate (gypsum) scale in nanofiltration of saline agricultural drainage water. *Environmental Engineering Science*, 19: 387–398.
23. Sutzkover, I., Hasson, D., and Semiat, R. (2000) Simple technique for measuring the concentration polarization level in a reverse osmosis system. *Desalination*, 131: 117–127.
24. Hoek, E.M.V., Kim, A.S., and Elimelech, M. (2002) Influence of cross-flow filter geometry and shear rate on colloidal fouling in reverse osmosis and nanofiltration separations. *Environmental Engineering Science*, 19: 357–372.
25. Wiesner, M.R. and Aptel, P. (1994) *Water Treatment Membrane Processes; McGraw Hill: Boston.*
26. Smith, R.M. and Martell, A.E. (2004) NIST Critically selected stability constants of metal complexes database version 8. National Institute of Standards and Technology: Gaithersburg, MD.
27. Bott, T.R. (1988) Crystallization and fouling–basic science and models. In Bott, T.R., Melo, L.F. and Bernardo, C.A. (eds): *Fouling Science and Technology*, 251–260.
28. Song, L. and Elimelech, M. (1995) Theory of concentration polarization in cross-flow Filtration. *Journal of Chemical Society*, 91: 3389–3398.